FINITE ELEMENT ANALYSIS OF THE FATIGUE PROPAGATION OF BIFURCATED CRACKS

Antonio Carlos de Oliveira Miranda
Luiz Fernando Martha
amiranda@tecgraf.puc-rio.br
lfm@tecgraf.puc-rio.br
Tecgraf - Computer Graphics Technology Group and
Civil Engineering Department
Pontifical Catholic University of Rio de Janeiro (PUC-Rio), Rua Marquês de São Vicente 225, Rio de Janeiro, RJ 22453-900, Brazil.
Marco Antonio Meggiolaro
Jaime Tupiassú Pinho de Castro
meggi@mec.puc-rio.br
jtcastro@mec.puc-rio.br
Mechanical Engineering Department
Pontifical Catholic University of Rio de Janeiro (PUC-Rio), Rua Marquês de São Vicente 225, Rio de Janeiro, RJ 22453-900, Brazil.

Abstract. *Fatigue crack kinking and bifurcation are well-known phenomena capable of inducing significant growth retardation or even crack arrest. However, symmetrically bifurcated crack models available in the literature cannot account for the propagation behavior observed in practice. In this work, specialized Finite Element (FE) and life assessment software are used to predict the reduction in the propagation rates in asymmetrically bifurcated cracks. The crack path and the associated stress intensity factors (SIF) of asymmetrically bifurcated cracks are numerically obtained for several bifurcation angles. A companion life assessment program is used to estimate the number of delay cycles associated with crack bifurcation, allowing for a better understanding of the influence of crack deflection in the propagation life of structural components.*

Keywords: *fatigue, crack bifurcation, growth retardation.*

1. INTRODUCTION

It is well known that fatigue cracks can significantly deviate from their Mode I growth direction due to the influence of overloads, multi-axial stresses, micro structural inhomogeneities such as grain boundaries and interfaces, or environmental effects, generating crack kinking **or** branching (Lankford, 1981), see Figure 1. A fatigue crack deviated from its nominal Mode I plane induces mixed-mode near-tip conditions even if the far-field stress is purely Mode I. For instance, as shown in Fig. 1, a pure Mode I stress intensity factor (SIF) K_I induces Modes I and II SIF k_1 and k_2 near the longer branch of a bifurcated crack and k_1' and k_2' near the shorter one. Since these SIF associated to deflected or branched fatigue cracks can be considerably smaller than that of a straight crack with the same projected length, such deviations can retard or even arrest the subsequent crack growth (Suresh, 1983). In addition, the fracture surface roughness generated by such deviations can also alter the crack closure level, leading to further perturbations on the crack propagation rates.

It is experimentally observed that very small differences between the crack branch lengths **b** and **c** are enough to cause the shorter branch to arrest as the larger one propagates, generally changing its curvature until reaching approximately its pre-overload SIF and growth direction and rate, see Figure 2. Therefore, although many branches can be developed along the main crack path, only the fastest branch continues to grow, while all others are brought to a stop due to its shielding effect. In addition, the crack growth is retarded. This typical propagation behavior has been observed in many structural components, e.g. on a branched crack on an aircraft wheel rim made of 2014-T6 aluminum alloy (Kosec, 2002).

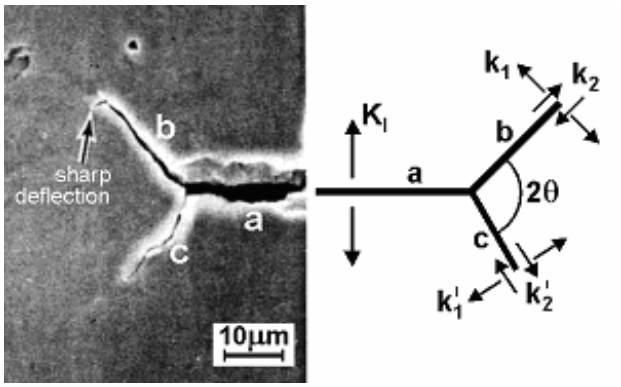

Figure 1 - Bifurcated crack geometry and nomenclature (Lankford, 1981).

Some analytical solutions have been obtained for the SIF of kinked and branched cracks, but it is generally recognized that it is very difficult to develop accurate analytical solutions to their complex propagation behavior (Suresh, 1993; Suresh, 1998; Seelig, 1999; Karihaloo, 1992). Therefore, presently numerical methods such as Finite Elements (FE) and Boundary Elements (BE) are the only practical means to predict the propagation behavior of branched cracks. A summary of such SIF solutions as a function of the deflection angle and the length of the deflected part of the crack are presented in Suresh (1986).

To predict the (generally curved) path of a branched crack and to calculate the associated Modes I and II SIF, a specially developed interactive FE program named Quebra2D (meaning 2D fracture in Portuguese) is used (Miranda, 2002). This program simulates two-dimensional fracture processes based on a FE self-adaptive strategy, using appropriate crack tip elements and crack increment criteria. The adaptive FE analyses are coupled with modern and very efficient automatic remeshing schemes. The remeshing algorithm developed for Quebra2D

works both for regions without cracks and for regions with one or multiple cracks, which may be either embedded or surface breaking.

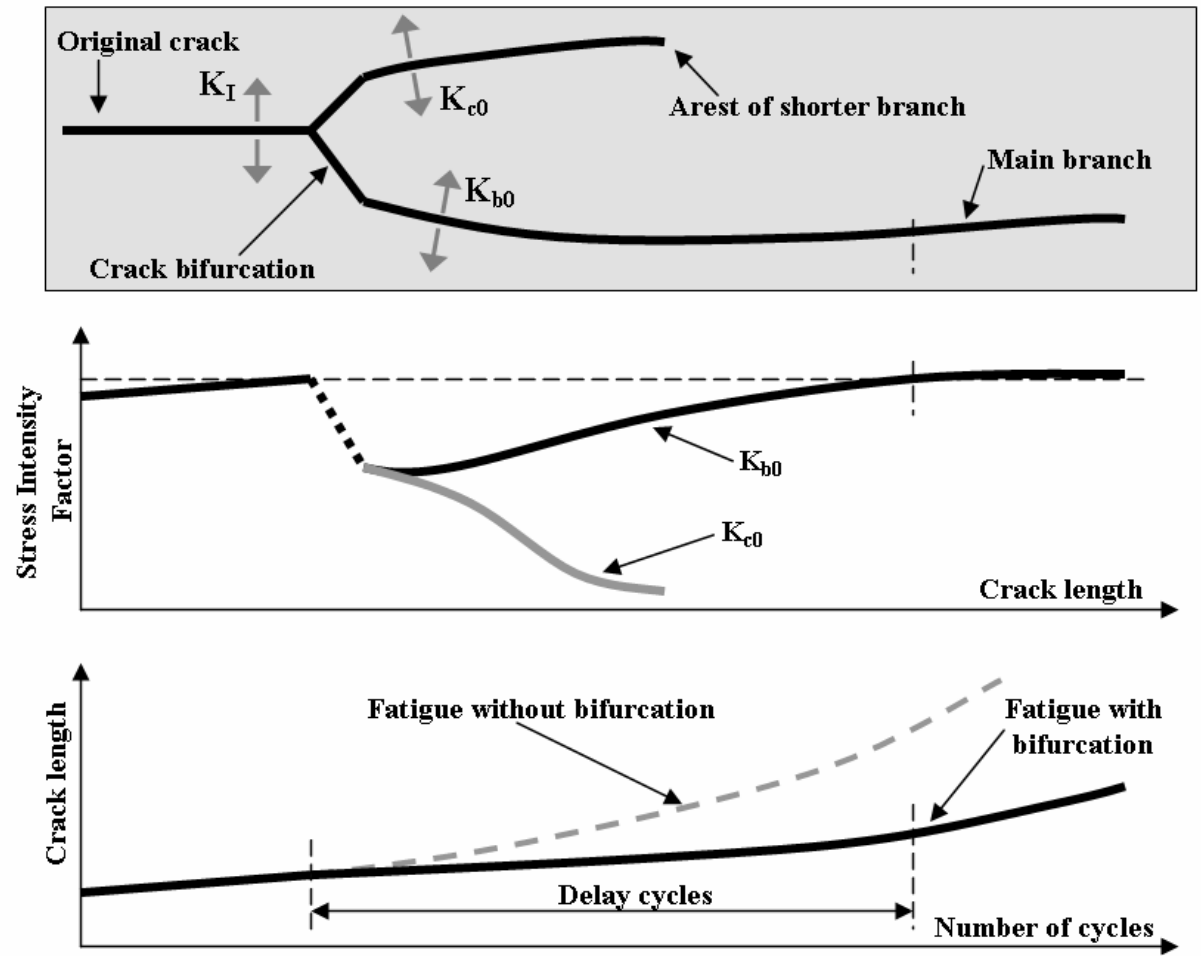

Figure 2 – Behavior of bifurcated crack propagation.

2. CRACK KINKING CALCULATIONS AND FINITE ELEMENT SOFTWARE VALIDATION

In this section, the Modes I and II SIF $\mathbf{k_1}$ and $\mathbf{k_2}$ are evaluated for cracks of length **a** with a small kink of length $\mathbf{b_0}$ at an angle q, see Figure 3(a). According to Bilby (1977) and Cotterell (1980), if $\mathbf{b_0}$ is much smaller than all other crack dimensions, then $\mathbf{k_1}$ and $\mathbf{k_2}$ can be calculated from the Modes I and II SIF $\mathbf{K_I}$ and $\mathbf{K_{II}}$ of the straight crack (without the kink) using:

$$\mathbf{k_1} = \frac{1}{4}\left(3\cos\frac{q}{2} + \cos\frac{3q}{2}\right)\mathbf{K_I} - \frac{3}{4}\left(\sin\frac{q}{2} + \sin\frac{3q}{2}\right)\mathbf{K_{II}} \quad (1)$$

$$\mathbf{k_2} = \frac{1}{4}\left(\sin\frac{q}{2} + \sin\frac{3q}{2}\right)\mathbf{K_I} + \frac{1}{4}\left(\cos\frac{q}{2} + 3\cos\frac{3q}{2}\right)\mathbf{K_{II}} \quad (2)$$

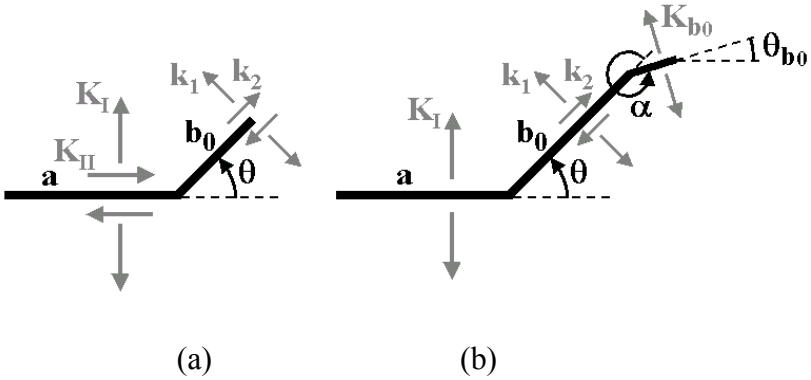

(a) (b)

Figure 3 - Schematic representation of a kinked crack before propagation (a) and at the onset of propagation (b).

Equations (1-2) are only valid for very small $\mathbf{b_0/a}$ ratios. On the other hand, when $\mathbf{b_0/a}$ is greater than **0.5**, $\mathbf{k_1}$ and $\mathbf{k_2}$ are also independent of $\mathbf{b_0/a}$ for both kinked and symmetrically bifurcated cracks.

To validate the Quebra2D program, the Modes I and II SIF $\mathbf{k_1}$ and $\mathbf{k_2}$ of an infinitesimally kinked crack ($\mathbf{b_0/a}$ ® **0** in Figure 3(a)) are obtained and compared to the analytical solutions.

In order to numerically reproduce Equations (1-2), very small $\mathbf{b_0/a}$ ratios must be considered. Kitagawa et al. (1975) performed numerical analyses using $\mathbf{b_0/a = 0.1}$, however this ratio was not small enough to converge to the infinitesimal kink solution. In this work, a standard C(T) specimen is FE modeled with width **w = 32.0mm**, crack length **a = 14.9mm**, and a very small kink with length $\mathbf{b_0}$ = **10**㎜. It is found that the considered ratio $\mathbf{b_0/a}$ = **10㎜/14.9mm = 6.7´10^{-4} << 0.1** is appropriate for this validation.

Note that an efficient meshing algorithm is fundamental to avoid elements with poor aspect ratio, since the ratio between the size scale of the larger and smaller elements is above 1,000 in this case. To accomplish that, Quebra2D uses an innovative algorithm incorporating a quadtree procedure to develop local guidelines to generate elements with the best possible shape. The internal nodes are generated simultaneously with the elements, using the quadtree procedure only as a node-spacing function. This approach tends to give a better control over the generated mesh quality and to decrease the amount of heuristic cleaning-up procedures. Moreover, it specifically handles discontinuities in the domain or boundary of the model. Finally, to enhance the quality of the shape of the mesh element, an *a posteriori* local mesh improvement procedure is used (Miranda, 1993).

Figure 4 shows a comparison between the analytical and the FE-predicted $\mathbf{k_1}$ and $\mathbf{k_2}$ (normalized by the straight crack SIF $\mathbf{K_I}$) for several kink angles q, showing a very good agreement. The equivalent SIF $\mathbf{K_{b0}}$, which is the crack rate controlling parameter, is then calculated based on the $\sigma_{\theta max}$ criterion (Miranda, 1993), using $\mathbf{K_I}$ ° $\mathbf{k_1}$ and $\mathbf{K_{II}}$ ° $\mathbf{k_2}$. This $\mathbf{K_{b0}}$ can also be interpreted as the Mode I SIF of the kinked crack immediately after it starts propagating, soon after the expected sharp deflection is developed. Note that $\mathbf{K_{b0}}$ is only significantly smaller than the straight crack $\mathbf{K_I}$ (e.g. beyond 5%) for kink angles larger than **45°**. Therefore, crack kinking is not a significant cause of retardation for kink angles smaller than **45°**.

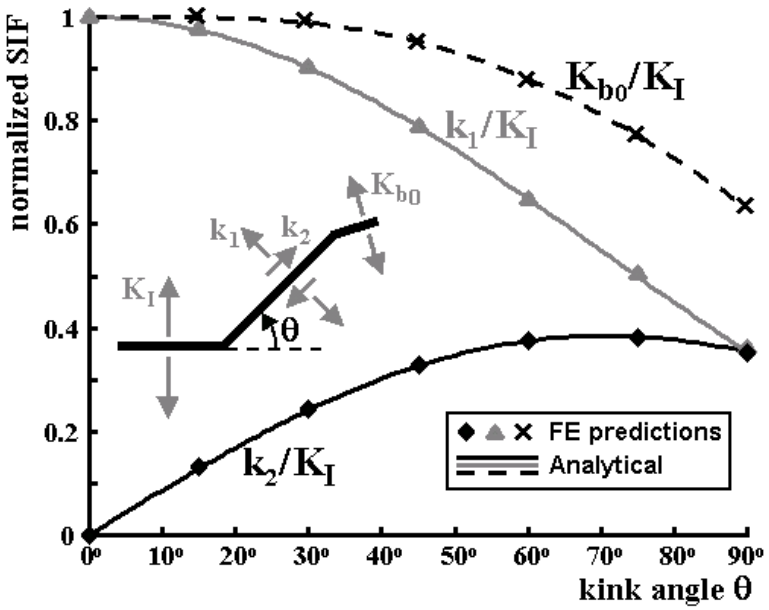

Figure 4 - Validation of the Quebra2D software for a kinked crack.

The equivalent SIF $\mathbf{K_{b0}}$ at the onset of the propagation can be calculated analytically using the s_{qmax} criterion, however its expression is quite lengthy, see Equation (3a), where sign(x) is the sign function returning either 1, 0 or −1. Alternatively, a simple and practical empirical function of q (in degrees) can be successfully fitted to the calculated data within less than **1%**, see Equation (3b).

$$\frac{K_{b0}}{K_I} = \frac{1}{16}\left(3\cos\frac{\theta_0''}{2}+\cos\frac{3\theta_0''}{2}\right)\left(3\cos\frac{\theta}{2}+\cos\frac{3\theta}{2}\right)+\frac{3}{16}\left(\sin\frac{\theta_0''}{2}+\sin\frac{3\theta_0''}{2}\right)\left(\sin\frac{\theta}{2}+\sin\frac{3\theta}{2}\right)$$

$$\theta_0'' = 2\arctan\left[\frac{1}{4}\cdot\frac{3\cos\theta/2+\cos3\theta/2}{\sin\theta/2+\sin3\theta/2}-\frac{1}{4}\cdot sign\left(\sin\frac{\theta}{2}+\sin\frac{3\theta}{2}\right)\cdot\sqrt{\left(\frac{3\cos\theta/2+\cos3\theta/2}{\sin\theta/2+\sin3\theta/2}\right)^2+8}\right] \quad (3a)$$

$$\frac{\mathbf{K_{b0}}}{\mathbf{K_I}} = \begin{cases} \mathbf{1}, & \text{if } q \le \mathbf{10^o} \\ \mathbf{1 - 0.37}\left(\dfrac{q - \mathbf{10^o}}{\mathbf{80^o}}\right)^{\mathbf{2.4}}, & \text{if } q > \mathbf{10^o} \end{cases} \quad (3b)$$

The initial propagation angle q_{b0}, defined in Figure 3(b), can also be calculated using the s_{qmax} criterion and fitted within less than **1%** by the empirical function:

$$q_{b0} = \begin{cases} \mathbf{0^o}, & \text{if } q \le \mathbf{10^o} \\ \mathbf{37^o}\left(\dfrac{q - \mathbf{10^o}}{\mathbf{80^o}}\right)^{\mathbf{1.7}}, & \text{if } q > \mathbf{10^o} \end{cases} \quad (4)$$

3. PROPAGATION OF BRANCHED CRACKS

The growth of branched cracks is studied in the Quebra2D program using the same C(T) specimen described above. A fixed crack growth step of D**b = 3**m**m** (or **1**m**m** during the first

propagation steps) is considered for the propagation of the longer branch **b**. This growth step is calculated in the direction defined by the s_{qmax} criterion. Due to the differences in the crack growth rate, a growth step D**c** smaller than D**b** is expected for the shorter branch. This smaller step is obtained assuming a crack propagation law that models the first two growth phases,

$$\frac{da}{dN} = A \times (\Delta K - \Delta K_{th})^m \tag{5}$$

where **A** and **m** are material constants and ΔK_{th} is the propagation threshold. If ΔK_b and ΔK_c are respectively the stress intensity ranges of the longer and shorter branches, then the growth step D**c** of the shorter branch **c** should be

$$\Delta c = \Delta b \times \left(\frac{\Delta K_c - \Delta K_{th}}{\Delta K_b - \Delta K_{th}}\right)^m \tag{6}$$

Interestingly, the ratio between the propagation rates of the two branches is independent of the material constant **A**. In this analysis, the exponent **m** is assumed to be **2.0**, **3.0**, and **4.0**, which are representative for the range of the measured exponents for steels. Note that a similar expression can be obtained if crack closure effects are considered, even including mean load effects through a function **f(R)** of the load ratio **R**, using the effective SIF $\Delta K_{eff} = K_{max} - K_{op}$:

$$\frac{da}{dN} = A \times (K_{max} - K_{op})^m \times f(R) \Rightarrow \Delta c = \Delta b \times \left(\frac{K_{max,c} - K_{op}}{K_{max,b} - K_{op}}\right)^m \tag{7}$$

where $K_{max,b}$ and $K_{max,c}$ are the maximum SIF of the longer and shorter branches respectively, and K_{op} is the crack opening SIF, assumed equal for both branches.

Once a (small) growth step D**b** is chosen for the numerical propagation of the longer branch, the growth of the shorter branch D**c** is readily obtained from Equations (6) or (7). Both the crack path and the associated SIF along each branch are then obtained using the FE program. Several numerical simulations were performed for different values of the exponent **m**, angle **2**q, relation c_0/b_0, and SIF, considering or not crack closure. Figure 5 shows the algorithm flowchart used to perform the analyses.

In the following sections, semi-empirical crack retardation equations are proposed to model the retardation effect along the path of the crack branches as a function of their ratio c_0/b_0, the bifurcation angle **2**q, and crack growth exponent **m**.

3. BRANCHED CRACK PROPAGATION WITHOUT CLOSURE

In this section, the propagation behavior of branched cracks is studied using FE considering no closure effects ($K_{op} = 0$). Figure 6 shows the contour plots of the normal stress component in the load direction axis and propagation results for a bifurcated crack with angle $2\theta = 150^o$, obtained from the FE analysis for $c_0/b_0 = 0.91$, $m = 2$ and no closure. In this figure, the deformations are highly amplified to better visualize the crack path. Note that the crack path deviates from the original branch angles, deflecting from $\pm 75^o$ to approximately $\pm 28^o$. In addition, the originally shorter branch arrests after propagating (only) about **29**m**m**, while the longer branch returns to the pre-overload growth direction and SIF (even though the subsequent crack growth plane may be offset from the pre-overload one, see Figure 6).

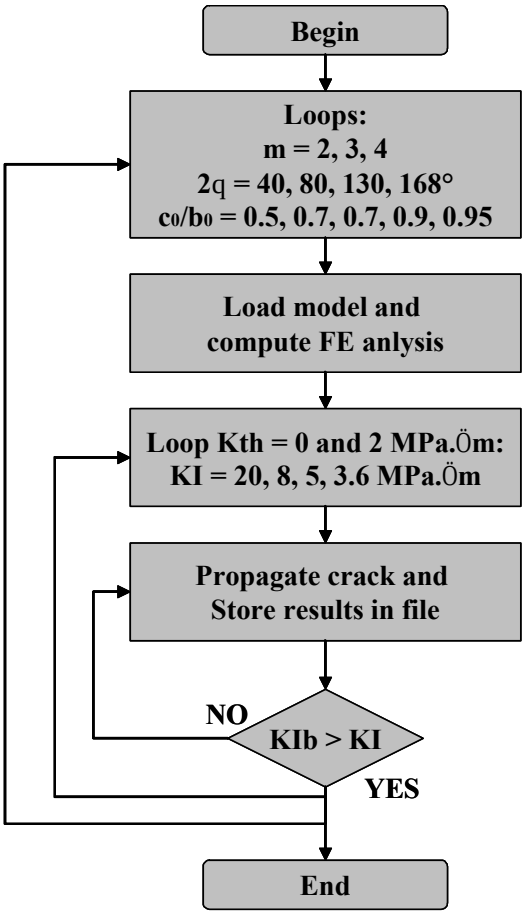

Figure 5 - Algorithm flowchart used to perform the analyses.

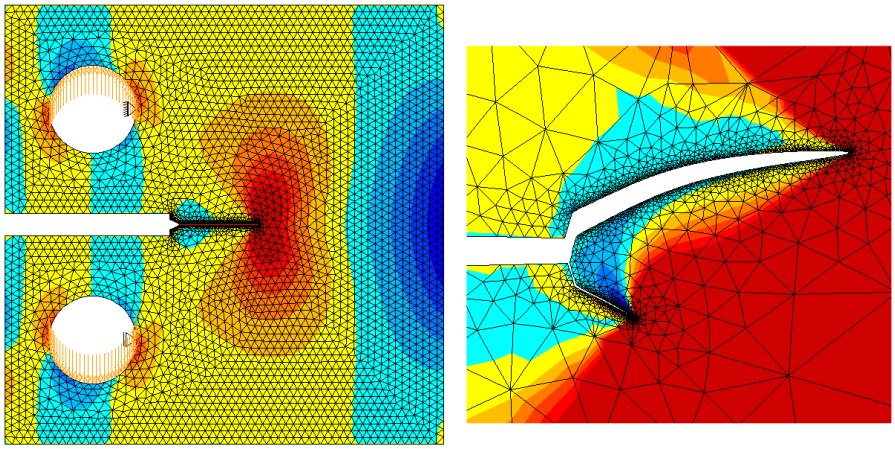

Figure 6 - Propagation simulation of a bifurcated crack on a C(T) specimen (left), and close-up view of the two original **11mm** and **10mm** branches with angle **2q = 150°** (right).

Figure 7 shows the crack paths obtained from the FE analyses of bifurcated cracks with **2q = 130°** and **c_0/b_0 = {0.5, 0.8, 0.95, 1}**, considering **m = 2** and no closure effects. The dashed lines show the theoretical propagation behavior of a perfectly symmetric bifurcation (**c_0/b_0 = 1**). In this case, the retardation effect would never end because both branches would

propagate symmetrically without arresting. Clearly, such behavior is not observed in practice, since the slightest difference between b_0 and c_0 would be sufficient to induce an asymmetrical behavior.

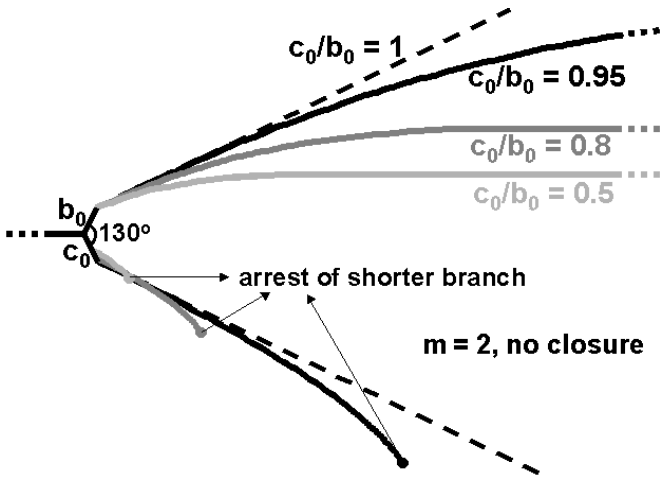

Figure 7 - Bifurcated crack paths for several $\mathbf{c_0/b_0}$ ratios.

The angles of the symmetrical dashed lines in Figure 7 for small $\mathbf{b_0/a}$ ratios are found to be $\mathbf{q^* = \pm 26.5^o}$ with respect to the horizontal, where $\mathbf{2q^*}$ has been previously defined as the bifurcation angle for which $\mathbf{k_2}$ vanishes on a symmetrically branched crack. As the symmetrical branches grow following the $\mathbf{\pm 26.5^o}$ directions, it is found that the ratio between the equivalent SIF and the SIF of a straight crack with same projected length is approximately constant and equal to **0.757**, a value compatible with the **0.75** estimate for $\mathbf{K_{b0}}$. Note that the directions $\mathbf{\pm 26.5^o}$ are independent of **2**q, **m**, and the closure level, therefore symmetrical bifurcations with any initial angle **2**q would tend to the self-similar solution $\mathbf{2q^* = 53^o}$ as long as the ratio **b/a** of the propagating branches is sufficiently small. FE calculations also showed that the slopes of the dashed lines are gradually decreased as both branches grow, resulting in angles $\mathbf{\pm 18^o}$ in the vicinity of **b/a = 0.025**, $\mathbf{\pm 16^o}$ close to **b/a = 0.1**, and $\mathbf{\pm 15.3^o}$ for **b/a >> 1**. This last result has been obtained from a FE analysis of a symmetrical bifurcation starting at the edge of a very large plate (therefore with **a = 0** and **b/a** ® ¥).

Figure 7 also shows that lower $\mathbf{c_0/b_0}$ ratios result in premature arrest of the shorter crack branch, leading to smaller retardation zones. Also, the propagation path of the longer branch is usually restrained to the region within the dashed lines, while the shorter one is "pushed" outside that envelope due to shielding effects.

The size of the retardation zone can be estimated from the ratio $\mathbf{b_f/b_0}$, where $\mathbf{b_f}$ is the value of the length parameter **b** of the longer branch beyond which the retardation effect ends (in the same way that it was defined for kinked cracks). The ratio $\mathbf{b_f/b_0}$ is then calculated through FE propagation simulations for all combinations of $\mathbf{c_0/b_0 = \{0.5, 0.8, 0.9, 0.95\}}$, $\mathbf{2q = \{40^o, 80^o, 130^o, 168^o\}}$ and $\mathbf{m = \{2, 3, 4\}}$, and fitted by the proposed empirical function:

$$\frac{\mathbf{b_f}}{\mathbf{b_o}} = \exp\left(\frac{\mathbf{2q - 30^o}}{\mathbf{56 + 17\,(m-2)^{2/3}}}\right) \Big/ \mathbf{(1 - c_0/b_0)^{(12-m)/20}} \qquad (8)$$

Figure 8 shows a comparison between the fitted and the FE-obtained data. Note that a greater symmetry between the branches (as $\mathbf{c_0/b_0}$ approaches **1.0**) results in a longer retardation zone, as expected from the delayed arrest of the shorter branch.

The FE-calculated equivalent SIF $\mathbf{K_b}$ and $\mathbf{K_c}$ of the longer and of the shorter branches are now evaluated along the obtained crack paths. Figures 9(a) and 9(b) plots the crack retardation factors (defined as the ratios between $\mathbf{K_b}$ or $\mathbf{K_c}$ and the Mode I SIF $\mathbf{K_I}$ of a straight crack) for $\mathbf{2q = 130^o}$ and $\mathbf{m = 2}$, as a function of the normalized length $\mathbf{(b - b_0)/b_0}$ of the longer branch (measured along the propagation path). Because of the different crack branch lengths, the SIF at the longer one is much higher than that at the shorter branch. Assuming $\mathbf{K_b}$ and $\mathbf{K_c}$ to be the crack driving force, it can be seen from Figures 9(a) and 9(b) that the longer branch reaches its minimum propagation rate right after the bifurcation occurs, returning to its pre-overload rate as the crack tip advances away from the influence of the shorter branch. As seen in the figure, the retardation behavior is misleadingly similar to closure-related effects, even though no closure is present in that case.

In addition, as the length difference between both branches increases, it is expected that the propagation rate of the shorter one is reduced until it arrests, after which the larger branch will dominate. Note that even small differences between the branch lengths, such as in the case $\mathbf{c_0/b_0 = 0.95}$ shown in Figures 9(a) and 9(b), are sufficient to cause subsequent arrest of the shorter branch.

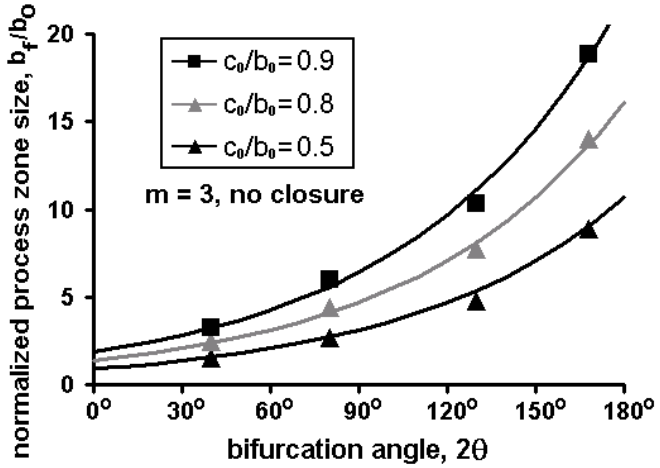

Figure 8 - Normalized process zone size as a function of the bifurcation angle and branch asymmetry $\mathbf{c_0/b_0}$ ($\mathbf{m = 3}$).

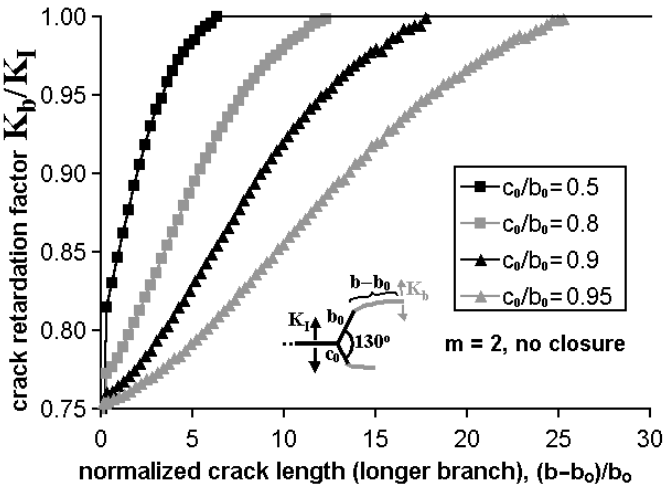

Figure 9(a) - Normalized equivalent SIF for the longer branch of a bifurcated crack during its propagation ($\mathbf{2q = 130^o}$, $\mathbf{m = 2}$).

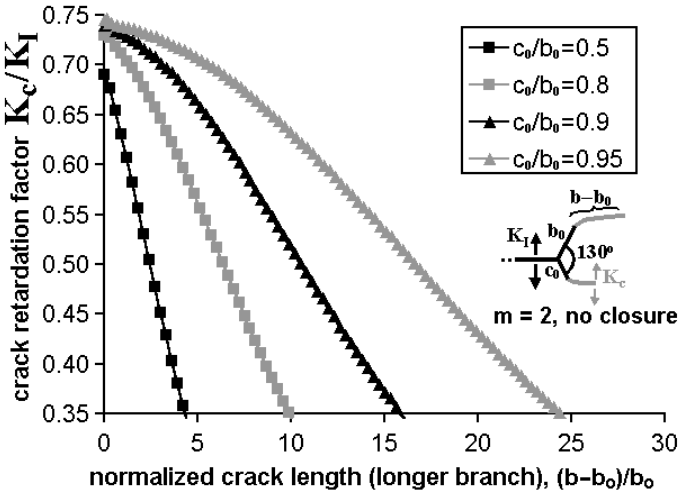

Figure 9(b) - Normalized equivalent SIF for the shorter branch of a bifurcated crack during its propagation (**2**q = **130°**, **m = 2**).

An empirical expression is here proposed to model the SIF $\mathbf{K_b}$ of the longer branch during the transition between $\mathbf{K_{b0}}$ (immediately after the bifurcation event) and the straight-crack $\mathbf{K_I}$ (after the end of the retardation effect), valid for $\mathbf{b_0 \le b \le b_f}$ and $\mathbf{0.7 < c_0/b_0 < 1}$:

$$\mathbf{K_b = K_{b0} + (K_I - K_{b0}) \left\{ atan\left(3 \frac{b - b_0}{b_f - b_0} \right) / 1.25 \right\}^{2c_0/b_0}} \tag{9}$$

where $\mathbf{b_f}$ is given in Equation (8) and $\mathbf{K_{b0}}$ by

$$\mathbf{\frac{K_{b0}}{K_I} = 0.75 + (1 - \sin q) \left(1 - \frac{c_0}{b_0} \right)} \tag{10}$$

It must be pointed out, however, that the presented FE results and empirical models might have some limitations, because actual bifurcations can be of a size comparable to the scale of the local plasticity (e.g., of the plastic zone size) or microstructural features (e.g., of the grain size). Moreover, possible closure and environmental effects should be considered when comparing the bifurcation model predictions with measured crack growth rates (Suresh, 1983). The interaction between crack branching and closure is studied next.

4. BRANCHED CRACK PROPAGATION WITH CLOSURE

All presented branched growth simulations so far have not included the effect of crack closure. This effect is easily accounted for in the FE calculations using Equation (7). The crack opening SIF $\mathbf{K_{op}}$ is assumed to be the same at both branch tips and always larger than the minimum SIF of each branch. Further simulations are then conducted considering several $\mathbf{K_{op}}$ values, normalized by the maximum Mode I SIF $\mathbf{K_I}$ of the straight crack, namely $\mathbf{K_{op}/K_I = \{0.067, 0.08, 0.10, 0.13, 0.20, 0.25, 0.40, 0.57\}}$.

A generalized version of Equation (8) is then proposed to fit the calculated process zone sizes including crack closure effects:

$$\frac{b_f}{b_o} = \frac{a}{(1 - c_0 / b_0)^{(12-m)/20}} \times \exp\left[\frac{-b}{(1 - c_0 / b_0)^{g}} \times \frac{K_{op}}{K_I}\right] \tag{11}$$

where

$$a = \exp\left[\frac{2q - 30^o}{56 + 17 \times (m - 2)^{2/3}}\right] \tag{12}$$

$$b = \left[\frac{2q}{110 + 60 \times (m - 2)^{0.6}}\right]^{5/2} \tag{13}$$

$$g = \frac{180^o - 2q}{280 - 130 \times (m - 2)^{0.3}} \tag{14}$$

Note that the ratio K_{op}/K_I in Equation (11) should be replaced with zero if K_{op} is smaller than the minimum SIF of both branches, because in this case the crack would remain opened during the entire cycle. Figures 10 and 11 show a comparison between the fitted and the FE-obtained data as a function of the crack opening ratio K_{op}/K_I. Note that greater closure levels result in shorter retardation zones, because the shorter branch is more easily arrested due to the reduction in its effective stress intensity range.

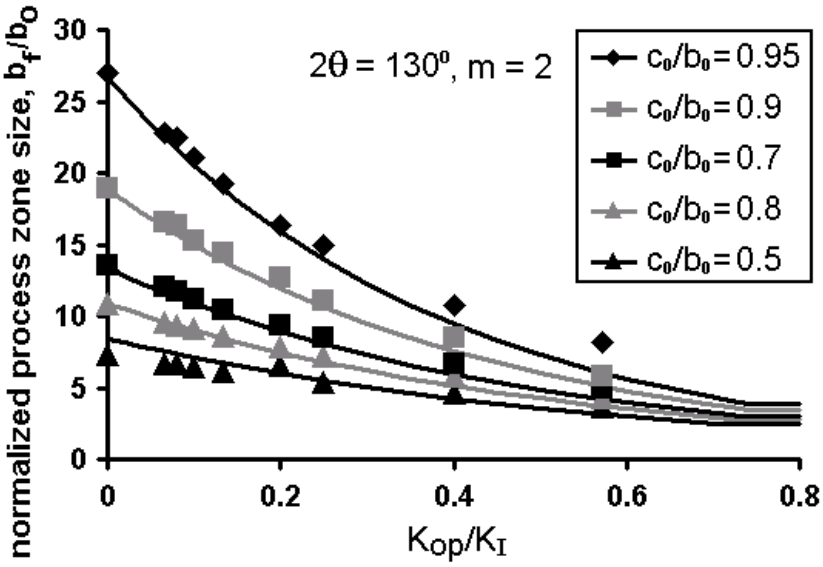

Figure 10 - Normalized process zone size of bifurcated cracks as a function of the crack opening SIF and branch asymmetry c_0/b_0 ($2q = 130^o$, $m = 3$).

Figure 12 shows the effect of crack closure at the branch tips on the retardation factor for $2q = 130^o$, $c_0/b_0 = 0.9$ and $m = 2$. Note that higher closure levels reduce the size of the retardation process zone, due to the closure-induced premature arrest of the shorter branch. In Figure 12, e.g., the normalized size of the process zone is reduced from **18** for no closure to **3.6** for $K_{op}/K_I = 0.74$, a factor of **5**. In this example, **0.74** is the minimum closure level that prevents the shorter branch to even start propagating. Therefore, at any closure level above

0.74 the normalized process zone size will also be **3.6**, because the propagation geometry will remain unchanged as long as the shorter branch remains at $\mathbf{c = c_0}$, as discussed before.

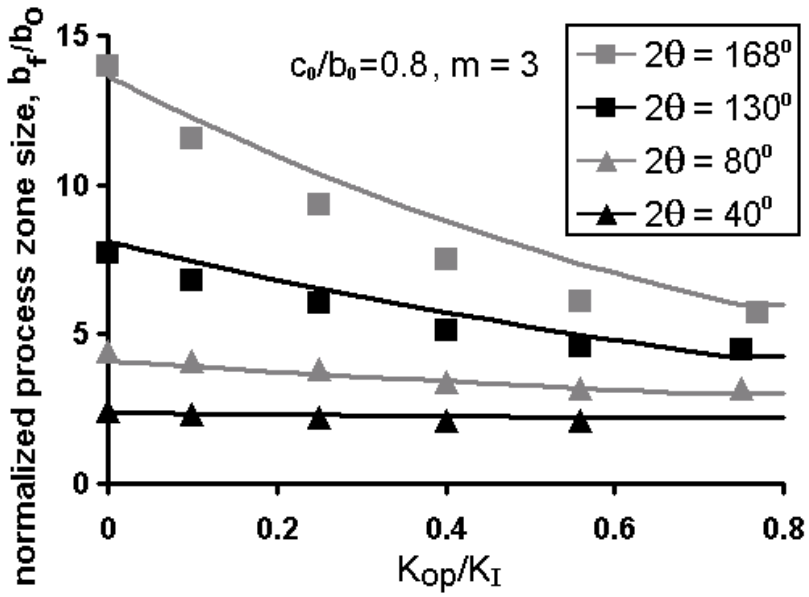

Figure 11 - Normalized process zone size of bifurcated cracks as a function of the crack opening SIF and bifurcation angle **2**q ($\mathbf{c_0/b_0 = 0.8}$, **m = 3**).

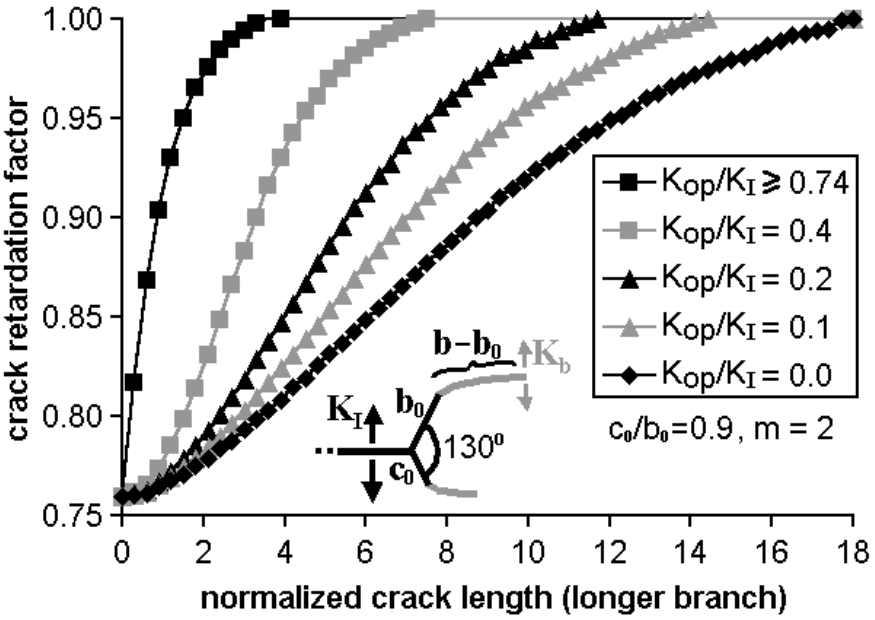

Figure 12 - Normalized SIF of the longer branch during its propagation as a function of the normalized length $\mathbf{(b - b_0)/b_0}$ for several opening levels ($\mathbf{c_0/b_0 = 0.9}$, **m = 2**).

Note, however, that a smaller process zone does not necessarily mean fewer delay cycles, since the longer branch will also experience a closure-induced reduction in the crack propagation rate. Therefore, a competition between lower growth rates of the longer branch and smaller process zone sizes will take place to determine the real effect of combined bifurcation and closure.

Equations (11-14) and (10) can then be applied to Equation (9) to model the SIF $\mathbf{K_b}$ of the longer branch during the transition between $\mathbf{K_{b0}}$ (the SIF immediately after the bifurcation event) and the straight-crack $\mathbf{K_I}$ (the SIF after the end of the retardation effect), completing this analysis.

5. CONCLUSION

In this work, a specialized FE program was used to calculate the propagation path and associated stress intensity factors (SIF) of kinked and bifurcated cracks, which can cause crack retardation or even arrest. A total of 262 crack propagation simulations were obtained from a total of 6,250 FE calculation steps to fit empirical equations to the process zone size and crack retardation factor along the curved crack path. In particular, the bifurcation simulations included several combinations of bifurcation angles $\mathbf{2\theta = \{40^o, 80^o, 90^o, 130^o, 168^o\}}$, branch asymmetry ratios $\mathbf{c_0/b_0 = \{0.5, 0.7, 0.8, 0.9, 0.95, 1.0\}}$, crack growth exponents $\mathbf{m = \{2, 3, 4\}}$, and even considered interaction between crack branching and closure effects through the ratios $\mathbf{K_{op}/K_I = \{0.0, 0.067, 0.08, 0.10, 0.13, 0.20, 0.25, 0.40, 0.57\}}$.

It was shown that very small differences between the lengths of the bifurcated branches are sufficient to cause the shorter one to eventually arrest as the longer branch returns to the pre-overload propagation conditions. The process zone size was found to be smaller for lower bifurcation angles and for branches with greater asymmetry, in both cases due to the increased shielding effects on the shorter branch. The retardation zone was reduced as well for materials with higher crack growth exponents, due to the increased difference between the crack growth rates of the longer and shorter branches. Higher closure levels also resulted in smaller process zones, because the shorter branch was more easily arrested due to the reduction in its effective stress intensity range. However, a competition between smaller process zone sizes and lower growth rates of the longer branch did take place to determine the real effect of combined bifurcation and closure.

The proposed equations, besides capturing all above described phenomena, can be readily used to predict the propagation behavior of branched and kinked cracks in an arbitrary structure, as long as the process zone is small compared to the other characteristic dimensions.

It should be recognized however that the presented mixed-mode equations are only accurate if the kink length greatly exceeds the size scale of the microstructural inhomogeneities and the size of the near-tip plastic zone. But assuming that the entire crack-front deflects uniformly, the specimen thickness itself may provide the size scale requirements for the validity of the presented equations, as the calculated SIF may be averaged considering the (several) grains present along the thickness. Otherwise, if the crack deflections vary significantly along the thickness, then further modeling including Mode III effects should be considered.

6. REFERENCES

Lankford, J., Davidson, D.L. “The Effect of Overloads upon Fatigue Crack Tip Opening Displacement and Crack Tip Opening/Closing Loads in Aluminum Alloys,” in Advances In Fracture Research, Pergamon Press, v.2, pp.899-906, 1981.

Suresh, S. “Crack Deflection: Implications for the Growth of Long and Short Fatigue Cracks,” Metallurgical Transactions, v.14a, pp.2375-85, 1983.

Kosec, B., Kovacic, G., Kosec, L. “Fatigue Cracking of an Aircraft Wheel,” Engineering Failure Analysis, v.9, pp.603-9, 2002.

Suresh, S. “Micromechanisms of Fatigue Crack Growth Retardation Following Overloads,” Engineering Fracture Mechanics, v.18, n.3, pp.577-93, 1983.

Suresh, S. “Fatigue of Materials,” ISBN 0-521-57847-7, Cambridge University Press, 1998, 679p.

Seelig, T., Gross, D. “On the Interaction and Branching of Fast Running Cracks - A Numerical Investigation,” Journal of the Mechanics and Physics of Solids, v.47, pp.935-52, 1999.

Karihaloo, B.L. “On Crack Kinking and Curving,” Mechanics of Materials, v.1, pp.189-201, 1982.

Miranda, A.C.O., Meggiolaro, M.A., Castro, J.T.P., Martha, L.F., Bittencourt, T.N. “Fatigue Crack Propagation under Complex Loading in Arbitrary 2D Geometries,” in Braun AA, McKeighan PC, Lohr RD, Editors, Applications of Automation Technology in Fatigue and Fracture Testing and Analysis, ASTM STP 1411, v.4, pp.120-46, 2002.

Kitagawa, H., Yuuki, R., Ohira, T. “Crack-Morphological Aspects in Fracture Mechanics,” Eng. Fracture Mechanics, v.7, pp.515-29, 1975.

Miranda, A.C.O., Meggiolaro, M.A., Castro, J.T.P., Martha, L.F., Bittencourt, T.N. “Fatigue Life and Crack Path Prediction in Generic 2D Structural Components”, Eng. Fracture Mechanics, v.70, pp.1259-79, 2003.